Nanoscale

Polymorphism of Low Dimensional Boron Nanomaterials Driven by Electrostatic Gating: A Computational Discovery

Journal:	*Nanoscale*
Manuscript ID	NR-ART-12-2019-010774.R1
Article Type:	Paper
Date Submitted by the Author:	21-Feb-2020
Complete List of Authors:	Jiao, Yalong; Queensland University of Technology; TU Dresden Ma, Fengxian; Hebei Normal University Gu, Jinxing; University of Puerto Rico, Rio Piedras Campus, Chen, Zhongfang; University of Puerto Rico, Department of Chemistry Du, Aijun; Queensland University of Technology, School of Chemistry, Physics and Mechanical Engineering

ARTICLE

Polymorphism of Low Dimensional Boron Nanomaterials Driven by Electrostatic Gating: A Computational Discovery

Received 00th January 20xx,
Accepted 00th January 20xx

DOI: 10.1039/x0xx00000x

Yalong Jiao,[a, d,*] Fengxian Ma,[a,c] Jinxing Gu,[b] Zhongfang Chen,[b,*] and Aijun Du[a,*]

The successful synthesis of two-dimensional (2D) boron sheets typically relies on the utilization of the silver surface, which acts as a gated substrate compensating the electron-deficiency of boron. However, how the structures of one-dimensional (1D) boron is affected by the gating effect remains unclear. By means of an unbiased global minimum structure search and density functional theory (DFT) computations, we discovered the coexistence of 2D boron sheets and 1D ribbons triggered by the electrostatic gating. Specifically, at low excess charge density level (<0.1 e/atom), 2D boron sheets dominate the low energy configurations. As the charge density increases (>0.3 e/atom), more 1D boron ribbons emerge, while the number of 2D layers is reduced. Additionally, a number of low-lying 1D boron ribbons were discovered, in which a flat borophene-like ribbon (FBR) was predicted to be stable and possess high mechanical strength. Moreover, the electride Ca_2N was identified as an ideal substrate for the fabrication of FBR because of its ability to supply a strong electrostatic field. This work bridges the gap between 2D and 1D boron structures, reveals the polymorphism of 1D boron ribbons under the electrostatic gating effect, and in general provides broad implications for future synthesis and applications of low-dimensional boron materials.

Introduction

Carbon is able to form robust in-plane sp^2 bonds, which is a key for the existence of stable, atomically thin, two-dimensional (2D) elemental material, i.e. graphene. As the lighter neighbour of carbon, boron displays more complicated bonding configurations, for example, planar or quasi-planar boron clusters[1] are stabilized by localized two-center–two-electron (2c–2e) σ bonds on the periphery as well as delocalized multicenter–two-electron (nc–2e) bonds in both σ and π frameworks.[2-4] Such bonding polymorphism endows boron with a variety of chemical and structural complexity in different dimensionalities.[5-16] However, three valence electrons of boron cannot completely occupy the in-plane sp^2 bonding state, consequently, the 2D hexagonal boron layers are electron-deficient, which significantly hinders the experimental preparation of 2D boron nanosheets.

To fabricate 2D boron, some effective strategies which can compensate boron's electron-deficiency have been proposed, such as applying electron-rich substrates,[17] introducing metal elements,[18-20] or chemical functionalization to form boron hydride nanosheets.[21] Encouragingly, two independent groups recently achieved the synthesis of 2D boron sheets (namely borophene, β_{12} and χ_3 boron sheets) on the silver substrate. [22, 23] The metal substrate not only supports the boron layers, but more importantly works as a gated substrate,[24] which induces the electron transfer from silver to the boron sheets, thus offsetting boron's deficiency and guiding boron's growth towards a stable 2D structure.[25, 26] Therefore, realizing a proper gate voltage on boron layers is crucial for the fabrication of low-dimensional boron materials.[27, 28] Specifically , Liu *et al* theotically investigated the charge doping effect for 2D boron layers, and discovered that two stable boron structures can be stabilized by placing on the electron-rich systems. [28]

2D boron sheets display many intriguing properties, such as high stiffness, low mass density, and high structural flexibility, for designing nanoelectronics.[29-35] In general, when the dimension of a material is reduced to one,[36, 37] the quantum confinement effect and surface/edge states endow one-dimensional (1D) nanostructures unique thermal, mechanical, electronic and optoelectronic properties.[38-43] For 1D boron, Liu *et al.*[44] theoretically predicted that two-atom wide ribbon and single-atom chain have rather high stabilities, and possess superior mechanical properties and structural flexibility trunable by strain, and Li *et al.*[7] predicted that the zigzag boron chains can be formed by the intercalation of tungsten (W) atoms. Nevertheless, the synthesis of 1D boron ribbons remains a grand challenge in experiments. Therefore, it is natural to ask how to realize the yet hypothetical 1D regime? Answering this question will not only facilitate the fabrication of 1D boron nanomaterials, but also benefit the development of other low-dimensional boron materials.

In this work, by means of evolutionary structure search and density functional theory (DFT) computations, we explored the entire configuration space of boron allotropes under excess electron conditions. Interestingly, we observed the coexistence of 2D and 1D

[a.] School of Physics and Chemistry and Centre for Materials Science, Queensland University of Technology, 2 George Street, Brisbane, QLD 4000 Australia.
E-mail: yalong.jiao@hdr.qut.edu.au; aijun.du@qut.edu.au
[b.] Department of Chemistry, University of Puerto Rico, Rio Piedras Campus, San Juan, PR 00931, United States.
E-mail: zhongfangchen@gmail.com
[c.] Department of Physics, Hebei Normal University, Shijiazhuang 050024, China
[d.] Theoretische Chemie, Technische Universität Dresden, Dresden 01062, Germany.
† Electronic Supplementary Information (ESI) available.

boron structures under the gating effect, and revealed the polymorphism of 1D boron configurations. At the charge density of 0.2 e/atom, a flat borophene-like ribbon (FBR) is found to be dynamically and thermally stable, and possesses high mechanical strength. Importantly, the electride Ca_2N layer was identified as an ideal substrate for the fabrication of 1D boron because it is able to supply a strong electrostatic field. Harnessing the formation of boron structures with different dimensions by gating effect provides a new strategy to further develop low-dimensional boron nanomaterials.

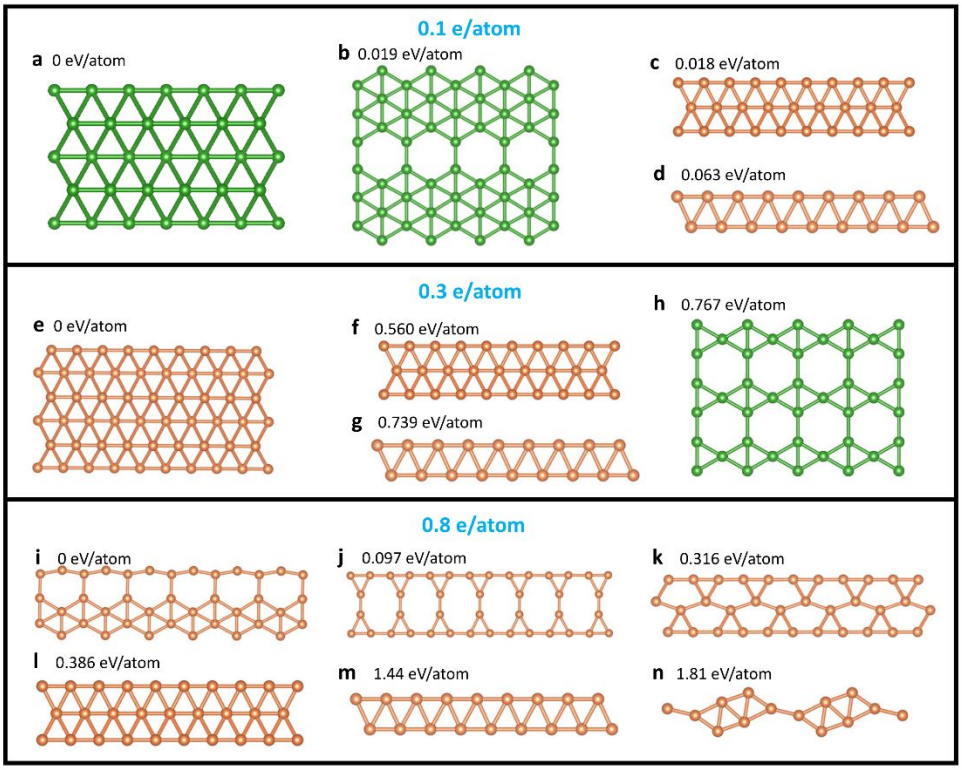

Figure 1 Top view and the energy per atom (En in eV/atom) of boron structures with the charge density of (a-d) 0.1, (e-h) 0.3, and (i-n) 0.8 e/atom, respectively. The 1D and 2D boron configurations are distinguished by orange and green colors, respectively.

Methods

Our structure search used the particle-swarm optimization (PSO) algorithm as implemented in the CALYPSO code.[45-48] The unit cell contains 6 atoms and the population size was set to 20, which is sufficient to reach convergence around the lowest-energy configurations on the potential energy surface. Each generation contains 20 structures, 60% of which are generated by PSO and the others are generated randomly. The subsequent structural relaxations were performed based on the density functional theory (DFT) using the generalized gradient approximation (GGA) in the form proposed by Perdew, Burke and Ernzerhof (PBE),[49] as implemented in the Vienna ab initio Simulation Package (VASP) code.[50, 51] The PBE functional has been confirmed to perform well for boron nanomaterials.[52] A plane-wave basis set with an energy cut-off of 400 eV was employed. A vacuum slab of about 15 Å was applied.

The structures were fully optimized until the maximum energy and force differences were less than 10^{-6} eV and 0.003 eV/Å, respectively. A Gamma-centered *k*-point mesh of $2\pi \times 0.03$ Å^{-1} was used for calculating electronic band structures. The phonon dispersion was computed on a 10 x 1 x 1 supercell for FBR by using the finite displacement method [53] as implemented in the Phonopy code. [54] In phonon calculations, the plane wave energy cut-off of 500 eV was employed with finer convergence criteria of energy (10^{-7} eV) and force (0.001 eV/Å).

The energies of charged structures were determined by DFT with the PBE functional as implemented in the CRYSTAL17 code.[55] The pob-TZVP basis sets[56] were used for the boron atom, where the fractional charge was added to the boron *p* orbital. Coulomb and exchange integral tolerance factors were set to tight values of 7, 7, 7, 7, and 14. The SCF convergence threshold for the total electron energy has been set to 10^{-7} a.u., and the shrinking factor of the irreducible Brillouin zone was set to 12.

Results and discussion

In the unbiased PSO search, a large population of boron structures were generated. The low-lying energy boron configurations at the charge-neutral state and with different levels of electron injection are summarized in the ESI (Fig. S1-S6). As a reference, we first performed the structure search for boron structures at the neutral condition, in which a number of planar or buckled 2D boron allotropes were produced, including P6/mmm boron sheet,[8] borophene,[22] β_3 and δ_5 sheet[57] (Fig. S1). Most of these 2D layers are of triangular lattices.

Then, we extended our structure search to investigate the low-lying boron nanostructures with extra negative charge density ranging from 0.1 e/atom to 0.8 e/atom. Further increasing the charge density from 0.8 to 1.0 e/atom generates rather similar structures. Thus, the charge density range of 0.1 -0.8 e is sufficient to describe the tendency of structure generation, and the results for 1.0 e/atom are not given for further discussion. The representative structures at the density level of 0.1 e/atom (approx. 4.33 x 10^{14} e/cm^2 experimentally) are shown in Fig. 1. Specifically, the lowest-energy 2D boron is the borophene layer (Fig. 1a), followed by planar β_3 boron sheet (Fig. 1b),[57] which composes of triangular boron lattices and hexagonal vacancies with a hole density d_h (defined as the hole number divided by the atom number in the triangular lattice) of 1/6. Interestingly, two 1D boron ribbons also emerge as the low-energy structures: a flat borophene-like ribbon (FBR, Fig. 1c), which can be also viewed as an infinite extension of B_7 cluster as building blocks;[58] closely followed by a two-atom-wide ribbon (TAR, Fig. 1d) with two zigzag boron atomic rows, which was recently predicted as the ground state 1D boron structure at charge-neutral state.[44] Especially, the energy of 1D FBR is 45 meV/atom lower than that of TAR. To sum up, at the very low charge density level of 0.1 e/atom, 1D boron nanostructures begin to emerge as competing alternatives of 2D boron sheets, and 1D and 2D forms are expected to coexist.

When the charge density increases to 0.3 e/atom (~ 1.30 x 10^{15} e/cm^2), more 1D structures, such as a buckled six-atom wide ribbon (Fig. 1e) and a truss-like ribbon (Fig. S4d), are revealed, while the number of low-energy 2D layers turns out to be reduced. Thus, at this charge density, the boron structures also favor to form 1D patterns. As the charge transfer further intensifies (0.5-0.8 e/atom, Fig. S5-S6), more 1D boron ribbons/chains join the low-energy structure list, while the 2D sheets become unfavorable. As shown in Fig. 1i – 1n, the 1D ribbons dominate the low-energy region, while no 2D forms are observed.

The coexistence of 2D and 1D boron structures triggered by the electric charge can be understood as follows. The four valence electrons per atom in graphene can fully occupy the in-plane sp^2 and out-of-plane p_z bonding state, thus forming a strong hexagonal pattern. However, such hexagonal configuration for 2D boron sheet (hexagonal boron sheet, HBS) is unstable, because boron's three valence electrons cannot fully occupy the sp^2 orbitals in this hexagonal two-centre bonding schceme.[59] Thus introducing excessive electrons into the boron layer is able to improve the stability of HBS. Triangular boron sheet (TBS) has a relatively lower energy due to its three-centre bonding state, but it is too electron-rich in occupying the anti-bonding states. Triangular boron framework with hexagonal vacancies (TBHV) properly mixes the two-centre and three-centre schemes, and has been proposed to be most stable because the electrons can fully fill the sp^2 bonding states while eliminate the anti-bonding occupation.[59, 60] The edge atoms in such TBHV act as 'acceptor' to accommodate the surplus of electrons, resulting in the highly improved stability in 2D TBHV. If the negative charge density increases in TBHV, the 'redundant' charges would fill more anti-bonding states, and thus enhance the Coulomb repulsion of boron atoms at the vacancy sites. Consequently, more edge atoms are required to store these 'redundant' charges and to stabilize the structure. Therefore, 1D boron ribbons featured with infinite 'edge atoms' are formed for extra charge accommodation. In other words, compared with 2D sheets, 1D ribbons can be easier to be stabilized under certain negatively charged conditions.

Our above analyses revealed that it is the charge density that determines the thermodynamically preferred dimensionalities of boron nanomaterials. Experimentally, introducing a gated substrate is a promising method to realize such excess charge density on the boron layer. In our case, the dimensionality control of boron structures should be able to be achieved by selecting proper substrates.

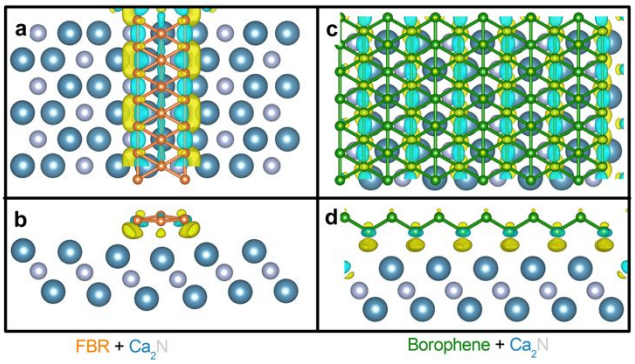

Figure 2 Top and side views of the charge density difference for (a-b) boron ribbon/Ca_2N and (c-d) borophene/Ca_2N complexes. Yellow and cyan iso-surfaces represent charge accumulation and depletion, respectively. The iso-value is set to 0.004 e/ Å^3.

Then, what substrate is appropriate to stabilize 1D boron nanomaterials relative to 2D boron nanosheets? To address this question, we computed the formation/binding energies of 2D borophene and its corresponding 1D analogue, namely FBR, on several substrates.

We first tested some well-known metal surfaces, such as Ag (1, 1, 1), Cu (1, 1, 1) and Al (1, 1, 1)[61] as potential substrates. However, 2D borophene has lower formation energy than 1D FBR on these metal substrates, thus is more favourable to grow. Since 1D boron ribbons are preferred when receiving sufficient charges, it is crucial to find an electron-abundant layer to induce substantial charge transfer from the substrate to the boron layer.

Under this guideline, the layered electride Ca_2N [62, 63] arises as a good choice, because its inherent ability to form a layer of delocalised electron gas and its nearly unparalleled power to supply a possibly adequate electrostatic field to the boron layer. To confirm this hypothesis, we chose a 2 x 2 boron sheet to match a 1 x 1 rectangular Ca_2N layer, in which the lattice mismatch is less than 4.6%. In the optimized ribbon + Ca_2N structure (Fig. 2a-2b), the borophene-like 1D FBR ribbon is slightly buckled. Encouragingly, on the Ca_2N layer, the boron ribbon has a lower formation energy (E_f = -6.339 eV/atom) than the 2D sheet (E_f = -6.248 eV/atom) (for details, see the ESI). By performing the Bader charge analysis, [64] we found that an average of 0.079 electrons per atom are transferred from the Ca_2N layer to the borophene layer. By contrast, more electrons

(0.136 e/atom) are transferred from the substrate to the FBR ribbon, indicating that the Ca_2N layer is an efficient electron donor to stabilize the 1D ribbons. Considering that the 2D planar β_3 boron sheet (Fig. 1b) is the second lowest energy 2D configuration at low charge level (0.1 e/atom), we also calculated the E_f for the β_3 boron sheet + Ca_2N complex (Fig. S7). Due to its strong electron coupling with the Ca_2N layer, β_3 sheet is buckled, and this system has a higher E_f (-6.280 eV/atom) than that of the boron ribbon. Thus, the Ca_2N layer is expected to be a good substract to favourably grow 1D boron ribbons.

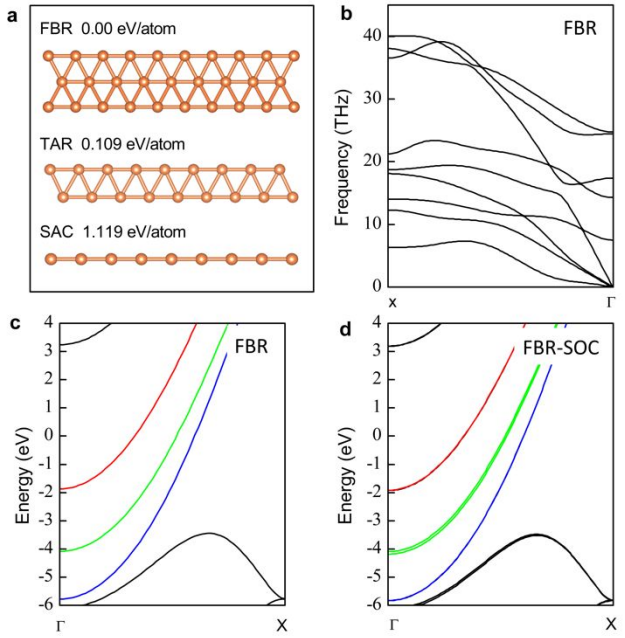

Figure 3 (a) Optimized structures of three 1D boron configurations with their relative energies (in eV/atom). (b) Phonon band dispersion and electronic band structures of FBR calculated by (c) HSE and (d) HSE+SOC method. The Femi level is set to zero.

To explore practical applications of freestanding 1D boron, it is significant to evaluate their stabilities and physical properties at charge-neutral state. Therefore, we examined three representative 1D boron nanostructures, including our newly predicted FBR as well as the previously reported TAR and single-atom chain (SAC),[44] and investigated their stabilities without additional charges. Notably, our newly discovered FBR has the lowest energy, which is 0.109 and 1.119 eV/atom lower in energy than TAR and SAC, respectively (Fig. 3a). We further evaluated the dynamic stability of FBR by calculating the phonon dispersion (Fig. 3b). Clearly, no imaginary frequency phonon exists at the wave vector, indicating this boron ribbon is dynamically stable. Additionally, our *ab* initio molecular dynamics (AIMD) simulations (Fig. S8- Fig. S9) showed that the structure of FBR is well preserved at the temperature up to 800 K after 10 ps simulations, suggesting its thermal stability at moderately high temperatures.

The unique high stability of 1D FBR prompted us to scrutinize its chemical bonding patterns[65] utilizing the Solid-sate adaptive natural density partitioning (SSAdNDP) method. [66-68] Each unit cell of 1D FBR has three boron atoms, thus nine valence electrons in total. To avoid the electrons-unpaired situation, we selected the supercell containing two unitcells as the chemical bonding search template, which contains 18 electrons. According to our analysis, there are four localized 2c-2e σ bonds in the edges of 1D FBR with the occupation numbers (ONs) of 1.77 |e| (Fig. 4a), four delocalized 3c-2e σ bonds with ONs of 1.81 |e| (Fig. 4b-4c), and one delocalized 7c-2e π bond with ONs of 1.95 |e| (Fig. 4d). The availability of the localized and delocalized multi-center σ bonds, and the delocalized multi-center π bonds significantly contributes to the high stability of this unique nanoribbon.

We further studied the mechanical properties of FBR by plotting the energy-strain curves (Fig. S10a). The tensile stiffness of this 1D boron is estimated as $P=\frac{1}{a}\frac{\partial^2 E_s}{\partial^2 \varepsilon}$, where a is the length of ribbon in one unit cell, E_s is the strain energy of a unit cell, and ε is the elastic strain. The estimated tensile stiffness for FBR (109.9 eV/ Å) is higher than those for TAR and SAC [44] (66.8 and 46.8 eV/ Å, respectively, this work) and carbyne.[69] The computed specific modulus, defined as P/d (d, the density of a material), of FBR is 4.49 x 10^8 NM/kg. This value is ca. 45% of the strongest carbon ribbon - carbyne (~10^9 NM/kg), demonstrating that FBR is relatively softer than carbyne per mass density. Poisson's ratio v reflects the mechanical responses of materials against external loads, and it can be described by calculating the relationship between the strain in *x*-direction and the corresponding deformation in *y*-direction.[70] The computed Poisson's ratio for FBR (0.286, Fig. S10b) is ca. 74% of that of carbyne (v= 0.386), indicating that FBR tends to have a smaller expansion/contraction (a less sensitive structural response) than carbyne in the transverse direction when subjected to a compressive/tensile strain in the longitudinal direction.

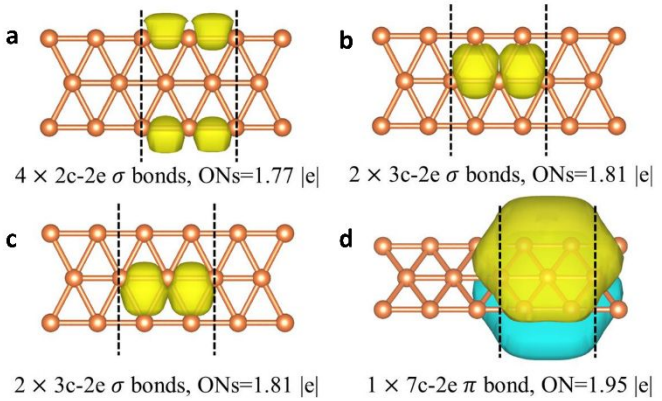

Figure 4 The SSAdNDP chemical bonding analysis of 1D FBR. (a) four 2c-2e σ bonds, (b) and (c) four 3c-2e σ bonds, besides (d) one 7c-2e π bond.

Then, we explored the electronic properties of boron ribbons in order to find practical applications of the emerging 1D boron nanostructures. FBR displays a metallic behaviour, and the high

parabolic slope at the Fermi level (Fig. 3c) implies the superior charge carrier mobility of this ribbon. If the edges of FBR were saturated by foreign atoms such as hydrogen, the band structure is not significantly affected (Fig. S11). When SOC is turned on, very weak magnetism appears in FBR with a value of 0.002 μB per unit cell. The magnetism in boron ribbon is weaker than that of the carbon ribbon.[71-73] Such small magnetism can hardly change the ground state of FBR and the energy differences among non-magnetic, ferromagnetic and antiferromagnetic state are negligible (< 10^{-6} eV). Though several bands show slight splitting in the SOC band structure of FBR (Fig. 3d), in general, the bands dispersions are similar with the non-SOC bands.

Possessing high stability, high tensile stiffness, and the lowest energy among 1D boron ribbons, FBR is promising for experimental fabrication and for the applications in mechanical and nannoelectronic devices. Furthermore, a four-atom wide ribbon with hexagonal holes FAR_{hex} displays linear band dispersion, and to our best knowledge, is first Dirac material discovered in 1D boron nanostructures (Fig. S12).

Conclusions

We performed ab initio evolutionary structure search for low-dimensional boron materials under excess charge density, and revealed the polymorphism of low dimensional boron materials driven by electrostatic gating. The predicted low-lying 1D boron ribbons are dynamically stable and energetically competitive to the previously reported boron ribbon/chain. Especially, a flat borophene-like ribbon is predicted to be of the lowest energy and have strong in-plane stiffness, making it promising in mechanical applications, and can be favourably grown on the experimentally available layered electride Ca_2N. This work highlights that the formation of boron configurations with different dimensionality can be controlled by the electrostatic gating, and provides a good guidance for future investigations of low dimensional boron materials.

Conflicts of interest

There are no conflicts to declare.

Acknowledgements

A.D. acknowledges the financial support by Australian Research Council under Discovery Project (DP170103598), and the computer resources provided by National Computational Infrastructure and the Pawsey Supercomputing Centre, which is supported by the Australian Government and the Government of Western Australia, through the National Computational Merit Allocation Scheme. Z.C. acknowledges the support by NSF-CREST Center for Innovation, Research and Education in Environmental Nano-technology (CIRE2N) (Grant Number HRD-1736093) and NASA (Grants 80NSSC17M0047). F.M. acknowledges the support from the National Natural Science Foundation of China (Grant No. 11847017 and 11904077) and Science Foundation of Hebei Normal University (Grant No. L2019B09).

Notes and references

1. W. An, S. Bulusu, Y. Gao and X. C. Zeng, *J. Chem. Phys.*, 2006, **124**, 154310.
2. A. P. Sergeeva, I. A. Popov, Z. A. Piazza, W.-L. Li, C. Romanescu, L.-S. Wang and A. I. Boldyrev, *Acc. Chem. Res.*, 2014, **47**, 1349-1358.
3. C.-C. Lee, B. Feng, M. D'Angelo, R. Yukawa, R.-Y. Liu, T. Kondo, H. Kumigashira, I. Matsuda and T. Ozaki, *Phys. Rev. B*, 2018, **97**, 075430.
4. I. A. Popov and A. I. Boldyrev, in *Boron*, Springer, 2015, pp. 1-16.
5. Z. Zhang, E. S. Penev and B. I. Yakobson, *Chem. Soc. Rev.*, 2017, **46**, 6746-6763.
6. F. Peng, M. Miao, H. Wang, Q. Li and Y. Ma, *J. Am. Chem. Soc.*, 2012, **134**, 18599-18605.
7. Q. Li, D. Zhou, W. Zheng, Y. Ma and C. Chen, *Phys. Rev. Lett.*, 2013, **110**, 136403.
8. F. Ma, Y. Jiao, G. Gao, Y. Gu, A. Bilic, Z. Chen and A. Du, *Nano Lett.*, 2016, **16**, 3022-3028.
9. A. J. Mannix, B. Kiraly, M. C. Hersam and N. P. Guisinger, *Nat. Rev. Chem.*, 2017, **1**, 0014.
10. X. Luo, J. Yang, H. Liu, X. Wu, Y. Wang, Y. Ma, S.-H. Wei, X. Gong and H. Xiang, *J. Am. Chem. Soc.*, 2011, **133**, 16285-16290.
11. J. O. C. Jiménez‐Halla, R. Islas, T. Heine and G. Merino, *Angew. Chem. Int. Ed.*, 2010, **49**, 5668-5671.
12. E. S. Penev, S. Bhowmick, A. Sadrzadeh and B. I. Yakobson, *Nano Lett.*, 2012, **12**, 2441-2445.
13. X. Yu, L. Li, X.-W. Xu and C.-C. Tang, *J. Phys. Chem. C*, 2012, **116**, 20075-20079.
14. A. A. Kistanov, Y. Cai, K. Zhou, N. Srikanth, S. V. Dmitriev and Y.-W. Zhang, *Nanoscale*, 2018, **10**, 1403-1410.
15. C. Zhang, T. He, S. K. Matta, T. Liao, L. Kou, Z. Chen and A. Du, *The Journal of Physical Chemistry Letters*, 2019, **10**, 2567-2573.
16. C. Tang, F. Ma, C. Zhang, Y. Jiao, S. K. Matta, K. Ostrikov and A. Du, *Journal of Materials Chemistry C*, 2019, **7**, 1651-1658.
17. Z. Zhang, Y. Yang, G. Gao and B. I. Yakobson, *Angew. Chem. Int. Ed.*, 2015, **54**, 13022-13026.
18. H. Zhang, Y. Li, J. Hou, K. Tu and Z. Chen, *J. Am. Chem. Soc.*, 2016, **138**, 5644-5651.
19. S. Ma, K. Bao, Q. Tao, C. Xu, X. Feng, P. Zhu and T. Cui, *Inorg. Chem.*, 2016, **55**, 11140-11146.
20. H. Tang and S. Ismail-Beigi, *Phys. Rev. B*, 2009, **80**, 134113.
21. Y. Jiao, F. Ma, J. Bell, A. Bilic and A. Du, *Angew. Chem. Int. Ed.*, 2016, **55**, 10292-10295.
22. A. J. Mannix, X.-F. Zhou, B. Kiraly, J. D. Wood, D. Alducin, B. D. Myers, X. Liu, B. L. Fisher, U. Santiago, J. R. Guest, M. J. Yacaman, A. Ponce, A. R. Oganov, M. C. Hersam and N. P. Guisinger, *Science*, 2015, **350**, 1513-1516.
23. B. Feng, J. Zhang, Q. Zhong, W. Li, S. Li, H. Li, P. Cheng, S. Meng, L. Chen and K. Wu, *Nat. Chem.*, 2016, **8**, 563-568.
24. Y. Li, K.-A. N. Duerloo, K. Wauson and E. J. Reed, *Nat. Commun.*, 2016, **7**, 10671.
25. R. Wu, A. Gozar and I. Božović, *npj Quantum Materials*, 2019, **4**, 40.
26. R. Wu, I. K. Drozdov, S. Eltinge, P. Zahl, S. Ismail-Beigi, I. Božović and A. Gozar, *Nature Nanotechnology*, 2019, **14**, 44-49.
27. Z. Zhang, S. N. Shirodkar, Y. Yang and B. I. Yakobson, *Angew. Chem. Int. Ed.*, 2017, **56**, 15421-15426.
28. D. Liu and D. Tománek, *Nano Lett.*, 2019, **19**, 1359-1365.
29. Z. Zhang, Y. Yang, E. S. Penev and B. I. Yakobson, *Adv. Funct. Mater.*, 2017, **27**, 1605059.
30. H. Zhang, Y. Xie, Z. Zhang, C. Zhong, Y. Li, Z. Chen and Y. Chen, *J. Phys. Chem. Lett.*, 2017, **8**, 1707-1713.
31. Z.-H. Cui, E. Jimenez-Izal and A. N. Alexandrova, *J. Phys. Chem. Lett.*, 2017, **8**, 1224-1228.
32. W.-c. Yi, W. Liu, J. Botana, L. Zhao, Z. Liu, J.-y. Liu and M.-s. Miao, *J. Phys. Chem. Lett.*, 2017, **8**, 2647-2653.
33. R. Zhang, Z. Li and J. Yang, *J. Phys. Chem. Lett.*, 2017, **8**, 4347-4353.
34. Y. Huang, S. N. Shirodkar and B. I. Yakobson, *J. Am. Chem. Soc.*, 2017, **139**, 17181-17185.
35. B. Feng, J. Zhang, S. Ito, M. Arita, C. Cheng, L. Chen, K. Wu, F. Komori, O. Sugino, K. Miyamoto, T. Okuda, S. Meng and I. Matsuda, *Adv. Mater.*, 2018, **30**, 1704025.
36. Q. Zhong, L. Kong, J. Gou, W. Li, S. Sheng, S. Yang, P. Cheng, H. Li, K. Wu and L. Chen, *Phys. Rev. Mater.*, 2017, **1**, 021001.
37. J. Tian, Z. Xu, C. Shen, F. Liu, N. Xu and H.-J. Gao, *Nanoscale*, 2010, **2**, 1375-1389.

38. Y. Xia, P. Yang, Y. Sun, Y. Wu, B. Mayers, B. Gates, Y. Yin, F. Kim and H. Yan, *Adv. Mater.*, 2003, **15**, 353-389.
39. V. Bezugly, J. Kunstmann, B. Grundkötter-Stock, T. Frauenheim, T. Niehaus and G. Cuniberti, *ACS Nano*, 2011, **5**, 4997-5005.
40. Y. Liu, Y.-J. Dong, Z. Tang, X.-F. Wang, L. Wang, T. Hou, H. Lin and Y. Li, *J. Mater. Chem. C*, 2016, **4**, 6380-6385.
41. W. Zhao, L. Wang, J. Bai, J. S. Francisco and X. C. Zeng, *Journal of the American Chemical Society*, 2014, **136**, 10661-10668.
42. X. Li, H. Lv, J. Dai, L. Ma, X. C. Zeng, X. Wu and J. Yang, *Journal of the American Chemical Society*, 2017, **139**, 6290-6293.
43. D. Yang, L. Luo, Y. Gao, S. Chen and X. C. Zeng, *Materials Horizons*, 2019, **6**, 1463-1473.
44. M. Liu, V. I. Artyukhov and B. I. Yakobson, *J. Am. Chem. Soc.*, 2017, **139**, 2111-2117.
45. Y. Wang, J. Lv, L. Zhu and Y. Ma, *Phys. Rev. B*, 2010, **82**, 094116.
46. Y. Wang, J. Lv, L. Zhu and Y. Ma, *Comput. Phys. Commun.*, 2012, **183**, 2063-2070.
47. Y. Wang, M. Miao, J. Lv, L. Zhu, K. Yin, H. Liu and Y. Ma, *J. Chem. Phys.*, 2012, **137**, 224108.
48. W. Yanchao, L. Jian, Z. Li, L. Shaohua, Y. Ketao, L. Quan, W. Hui, Z. Lijun and M. Yanming, *J. Phys. Condens. Matter*, 2015, **27**, 203203.
49. J. P. Perdew, K. Burke and M. Ernzerhof, *Phys. Rev. Lett.*, 1996, **77**, 3865-3868.
50. G. Kresse and J. Furthmüller, *Phys. Rev. B*, 1996, **54**, 11169-11186.
51. G. Kresse and J. Furthmuller, *Comput. Mater. Sci.*, 1996, **6**, 15-50.
52. F. Li, P. Jin, D.-e. Jiang, L. Wang, S. B. Zhang, J. Zhao and Z. Chen, *J. Chem. Phys.*, 2012, **136**, 074302.
53. K. Parlinski, Z. Q. Li and Y. Kawazoe, *Phys. Rev. Lett.*, 1997, **78**, 4063-4066.
54. A. Togo, F. Oba and I. Tanaka, *Phys. Rev. B*, 2008, **78**, 134106.
55. R. Dovesi, A. Erba, R. Orlando, C. M. Zicovich-Wilson, B. Civalleri, L. Maschio, M. Rérat, S. Casassa, J. Baima, S. Salustro and B. Kirtman, 2018, **8**, e1360.
56. M. F. Peintinger, D. V. Oliveira and T. Bredow, 2013, **34**, 451-459.
57. X. Wu, J. Dai, Y. Zhao, Z. Zhuo, J. Yang and X. C. Zeng, *ACS Nano*, 2012, **6**, 7443-7453.
58. I. Boustani, *Phys. Rev. B*, 1997, **55**, 16426-16438.
59. H. Tang and S. Ismail-Beigi, *Phys. Rev. Lett.*, 2007, **99**, 115501.
60. X. Yang, Y. Ding and J. Ni, *Phys. Rev. B*, 2008, **77**, 041402.
61. W. Li, L. Kong, C. Chen, J. Gou, S. Sheng, W. Zhang, H. Li, L. Chen, P. Cheng and K. Wu, *Science Bulletin*, 2018, **63**, 282-286.
62. K. Lee, S. W. Kim, Y. Toda, S. Matsuishi and H. Hosono, *Nature*, 2013, **494**, 336.
63. A. Walsh and D. O. Scanlon, *J. Mater. Chem. C*, 2013, **1**, 3525-3528.
64. G. Henkelman, A. Arnaldsson and H. Jónsson, *Comput. Mater. Sci.*, 2006, **36**, 354-360.
65. I. A. Popov, K. V. Bozhenko and A. I. J. N. R. Boldyrev, *Nano Research*, 2012, **5**, 117-123.
66. D. Y. Zubarev and A. I. Boldyrev, *Phys. Chem. Chem. Phys.*, 2008, **10**, 5207-5217.
67. B. D. Dunnington and J. R. Schmidt, *J. Chem. Theory Comput.*, 2012, **8**, 1902-1911.
68. T. R. Galeev, B. D. Dunnington, J. R. Schmidt and A. I. Boldyrev, *Phys. Chem. Chem. Phys.*, 2013, **15**, 5022-5029.
69. M. Liu, V. I. Artyukhov, H. Lee, F. Xu and B. I. Yakobson, *ACS Nano*, 2013, **7**, 10075-10082.
70. Y. Wang, F. Li, Y. Li and Z. Chen, *Nat. Commun.*, 2016, **7**, 11488.
71. L. Pisani, J. A. Chan, B. Montanari and N. M. Harrison, *Physical Review B*, 2007, **75**, 064418.
72. Y.-W. Son, M. L. Cohen and S. G. Louie, *Nature*, 2006, **444**, 347-349.
73. Y.-W. Son, M. L. Cohen and S. G. Louie, *Physical Review Letters*, 2006, **97**, 216803.

We discovered the structural diversity of 2D boron sheets and 1D ribbons triggered by the electrostatic gating.